Finite-temperature Dicke phase transition of a Bose-Einstein condensate in an optical cavity

Yuanwei Zhang,[1,2,*] Jinling Lian,[1,2,†] J.-Q. Liang,[1] Gang Chen,[2,‡] Chuanwei Zhang,[3] and Suotang Jia[2]

[1]*Institute of Theoretical Physics, Shanxi University, Taiyuan 030006, People's Republic of China*

[2]*State Key Laboratory of Quantum Optics and Quantum Optics Devices, Laser Spectroscopy Laboratory, Shanxi University, Taiyuan 030006, People's Republic of China*

[3]*Department of Physics and Astronomy, Washington State University, Pullman, Washington 99164, USA*

(Received 22 February 2012; revised manuscript received 16 October 2012; published 16 January 2013)

In this paper we investigate the finite-temperature properties of a Bose-Einstein condensate (BEC)-cavity system with a strong nonlinear atom-photon interaction by means of a functional path-integral approach. It is shown that the experimentally observed phase diagram [Baumann, Guerlin, Brennecke, and Esslinger, Nature (London) **464**, 1301 (2010)] can be better explained in our finite-temperature theory. More importantly, we identify a new dynamical unstable phase in this experiment. By tuning various experimental parameters, we reveal some rich temperature-driven phase diagrams and, in particular, predict a four-phase coexistence point. Finally, we find analytically that the specific heat in the superradiant phase increases exponentially at lower temperatures. Moreover, it has a large jump at the temperature-driven critical point where the superradiant-normal phase transition occurs. As a result, we argue that the specific heat can serve as a powerful tool to probe the thermodynamic properties of the BEC-cavity system.

DOI: 10.1103/PhysRevA.87.013616 PACS number(s): 37.30.+i, 05.30.Rt, 03.75.Hh, 42.50.Pq

I. INTRODUCTION

The experimental combination of a Bose-Einstein condensate (BEC) with a high-finesse optical cavity [1,2] opens new frontiers since it not only generates rich many-body phenomena of quantum gases [3–14] but also has potential applications in quantum information and quantum simulation [15,16]. For example, this hybrid system can allow us to explore the well-known Dicke model with infinite long-range interactions [17]. In this model, a second-order quantum phase transition from a superradiant phase (SP) to a normal phase (NP) was predicted more than 30 years ago [18–20]. However, the experimental observation is still challenging because the critical condition, i.e., the atom-photon coupling strength should be of the same order as the atomic resonant frequency, is hard to satisfy [21–24]. Recently, the superradiant quantum phase transition has been observed successfully in the BEC-cavity system by introducing the momentum-dependent spin states [25,26]. In fact, those pioneer experiments produce a generalized Dicke model with a nonlinear atom-photon interaction, which results from the light shift of a single maximally coupled atom. This nonlinear atom-photon interaction plays an important role in the self-organization of the ultracold atoms, and moreover, it also generates a positive feedback to suppress the density fluctuations. In the strong nonlinear interaction regime, rich dynamical properties as well as new quantum phase transitions have been predicted [27–29].

Physically, a quantum phase transition occurs at absolute zero temperature [30]. However, any experimental system is preformed at a finite temperature. For example, the temperature in Ref. [25] for observing the Dicke phase transition is ∼50 nK. More importantly, thermal fluctuations may induce new exotic phenomena beyond the predictions of the zero-temperature theory [31]. A well-known example is the loss of long-range superfluid order in low dimensions (two or one) at any temperature [32], where the superfluid physics is characterized by the Berezinskii-Kosterlitz-Thouless transition [33,34]. Thus, it is crucially important to investigate the thermodynamic properties of the system to fully understand the experimental findings as well as to explore further the temperature-dependent fundamental physics.

In this paper, we present an imaginary-time functional path-integral approach to study the finite-temperature properties of the recent experiment about the BEC-cavity system with the strong atom-photon nonlinear interactions [25]. Our main findings are the following:

(i) The experimentally observed phase diagram, i.e., Fig. 5 in Ref. [25], can be better explained in our finite-temperature theory. More interestingly, we show that a phase called the dynamical unstable phase (DUP) can be identified in this experiment.

(ii) Different from the known results of the original Dicke model, in which only the SP and the NP emerge at either zero or finite temperatures [18–20], we find rich thermodynamic phase diagrams including the NP, the SP, the CE_{NP} (coexistence of the stable NP and the metastable SP), and the DUP. In certain parameter regions, a temperature-induced four-phase coexistence point is predicted.

(iii) We show both analytically and numerically that the specific heat in the SP increases exponentially at lower temperatures. Moreover, it has a large jump at the critical temperature where the system has a transition from the SP to the NP. Therefore the specific heat may serve as a powerful tool to detect this temperature-driven phase transition.

This paper is organized as follows. In Sec. II, the model and the Hamiltonian for the experimental setup of the BEC-cavity system are illustrated briefly. In Sec. III, the thermodynamic equilibrium equation is obtained by means of the imaginary-time functional path-integral approach. The rich phase diagrams including the experimental observation are discussed in Sec. IV. The specific heats in the different phases are calculated in Sec. V. Finally, the conclusions are given in Sec. VI.

*zywznl@163.com

†myby1009@gmail.com

‡Corresponding author: chengang971@163.com

 ©2013 American Physical Society

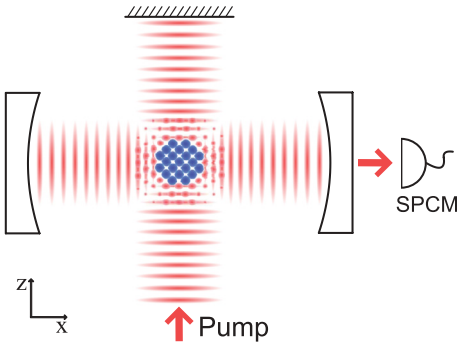

FIG. 1. (Color online) A BEC interacts strongly with a high-finesse optical cavity. The pump laser creates a standing-wave potential along the z direction. Within the combining pump-cavity mode profile, the ultracold atoms can coherently scatter pump light into the cavity mode with a position-dependent phase. In addition, the device single photon counting module (SPCM) is used to measure the mean-photon number in experiment.

II. MODEL AND HAMILTONIAN

Figure 1 shows the experimental scheme of the BEC-cavity system employed in Esslinger's group [25]. In contrast to previous proposals [22,23], this experiment prepares the momentum-dependent spin states $|\uparrow\rangle \equiv |p_x = \pm k, p_z = \pm k\rangle$ and $|\downarrow\rangle \equiv |p_x = 0, p_z = 0\rangle$, where p_x and p_z are the atomic momenta in the x and z directions. These pseudospin states can help us overcome the "no-go theorem," which rules out the SP-NP phase transition [35,36]. In the representation of these pseudospin states, the collective spin operators are defined as $S_x = \sum_i(|\uparrow_i\rangle\langle\downarrow_i| + |\downarrow_i\rangle\langle\uparrow_i|)$ and $S_z = \sum_i(|\uparrow_i\rangle\langle\uparrow_i| - |\downarrow_i\rangle\langle\downarrow_i|)$, and the corresponding Hamiltonian for the BEC-cavity system is written as ($\hbar = 1$) [25]

$$H = \left(\omega + \frac{U}{2N}S_z\right)\psi^\dagger\psi + \frac{\omega_0}{2}S_z + \frac{g}{\sqrt{N}}(\psi + \psi^\dagger)S_x, \quad (1)$$

where $\psi^\dagger$ denotes the photon creation operator. $\omega = -\Delta_c + 5U/2$ is the effective cavity frequency, where $\Delta_c = \omega_p - \omega_c$ is the pump-cavity detuning and $U = NU_0/4$ is the nonlinear atom-photon interaction [37]. $U_0 = g_0^2/(\omega_p - \omega_a)$ is the light shift of a single maximally coupled atom. ω_c is the cavity frequency, ω_a is the atomic transition frequency, ω_p is the pump laser frequency, and g_0 is the single atom-photon coupling strength. In experiment, both the pump laser and the cavity are red-detuning from the atomic D_2 line, so U is negative. However, both signs of U can be achieved. The effective atomic frequency is twice the atomic recoil energy $\omega_r = k^2/2m$, i.e., $\omega_0 = 2\omega_r$. $g = g_0\Omega\sqrt{N}/[2(\omega_p - \omega_a)]$ is the collective coupling strength, where Ω denotes the effective Rabi frequency tuned via the pump power.

III. THERMODYNAMIC EQUILIBRIUM EQUATION

The finite-temperature properties of the BEC-cavity system can be investigated by calculating the partition function or the free energy of Hamiltonian (1) using the imaginary-time ($\tau = it$) functional path-integral approach. By rewriting the collective spin operators as $S_x = \sum_{i=1}^N(\alpha_i^\dagger\gamma_i + \gamma_i^\dagger\alpha_i)$ and $S_z = \sum_{i=1}^N(\alpha_i^\dagger\alpha_i - \gamma_i^\dagger\gamma_i)$, where $\alpha_i^\dagger(\alpha_i)$ and $\gamma_i^\dagger(\gamma_i)$ are Fermi operators, the partition function is given by Ref. [38]

$$Z = \int [d\eta]\exp(-S), \quad (2)$$

where $[d\eta]$ is the integration measure. In the basis of $\Phi_i(\tau) = [\alpha_i(\tau), \gamma_i(\tau)]^T$, the action of Eq. (2) is expressed as

$$S = S_0 + \sum_{i=1}^N \int_0^\beta d\tau \Phi_i^\dagger(\tau) M \Phi_i(\tau), \quad (3)$$

where

$$S_0 = \int_0^\beta d\tau \psi^*(\tau)(\partial_\tau + \omega)\psi(\tau) \quad (4)$$

and

$$M = \partial_\tau I + \left(\frac{\omega_0}{2} + \frac{U}{2N}\psi^*\psi\right)\sigma_z + \frac{g}{\sqrt{N}}(\psi^* + \psi)\sigma_x, \quad (5)$$

where $\partial_\tau = \partial/\partial\tau$, $\beta = 1/(k_B T)$, I is the unit matrix, and σ_x and σ_z are the Pauli matrices.

Equation (2) shows that the partition function depends on both the boson field $\psi(\tau)$ and the Fermi field $\Phi_i(\tau)$. We first integrate over the Fermi field $\Phi_i(\tau)$ and obtain an effective action [39]:

$$S_{\text{eff}} = \int_0^\beta d\tau[\psi^*(\tau)(\omega + \partial_\tau)\psi(\tau) - N\text{Tr}\ln M]. \quad (6)$$

Furthermore, we can expand the effective action S_{eff} in Eq. (6) around the stationary points, in which the following equations

$$\frac{\delta S_{\text{eff}}(\psi^*, \psi)}{\delta\psi(\tau)} = \frac{\delta S_{\text{eff}}(\psi^*, \psi)}{\delta\psi^*(\tau)} = 0 \quad (7)$$

are satisfied, namely,

$$\begin{aligned}(\omega + \partial\tau)\psi^* &= (\omega + \partial\tau)\psi \\ &= -\frac{\left(\frac{\omega_0}{2} + \frac{U}{2N}\psi^*\psi\right)U\psi + 2g^2(\psi + \psi^*)}{\partial\tau^2 - \left[\left(\frac{\omega_0}{2} + \frac{U}{2N}\psi^*\psi\right)^2 + 4\frac{g^2}{N}\psi^*\psi\right]}.\end{aligned} \quad (8)$$

Equations (8) are the operator-dependent equations, which cannot be solved directly. In order to overcome this problem, we present the Fourier expansions for both the boson field and the Fermi field, i.e.,

$$\psi(\tau) = \beta^{-1/2}\sum_f \psi(f)e^{-if_n\tau}, \quad (9)$$

$$\Phi_i(\tau) = \beta^{-1/2}\sum_p \Phi_i(p)e^{-ip_n\tau}. \quad (10)$$

Since the boson field $\psi(\tau)$ and the Fermi field $\Phi_i(\tau)$ obey periodic and antiperiodic boundary conditions, respectively, we have $f_n = 2n\pi/\beta$ and $p_n = (2n+1)\pi/\beta$ with n being the integer number. Moreover, here we focus on the constant path that ψ is not influenced by τ. It implies that we can use the constant trajectories ($f = 0$) to obtain

$$\begin{aligned}\omega\psi^* &= \omega\psi \\ &= -\frac{1}{\beta}\sum_n \frac{\left(\frac{\omega_0}{2} + \frac{U}{2N}\psi^*\psi\right)U\psi^* + 2g^2(\psi + \psi^*)}{(-ip_n)^2 - \left[\left(\frac{\omega_0}{2} + \frac{U}{2N}\psi^*\psi\right)^2 + 4\frac{g^2}{N}\psi^*\psi\right]}.\end{aligned} \quad (11)$$

Finally, we consider the complex integration over the closed contours to calculate the infinite sums in Eq. (11). By means of the known result that $\sum_n F(ip_n)/\beta$ is equal to the sum of residues of $F(p)f(p)$ at poles of $F(p)$, where $f(p) = (1+e^{\beta p})^{-1}$ is the Fermi distribution [40], we obtain the thermodynamic equilibrium equation

$$\omega\psi = F(\psi^*,\psi)\tanh[\beta G(\psi^*,\psi)]\psi, \tag{12}$$

where

$$F(\psi^*,\psi) = \frac{\chi U + 4g^2}{2\sqrt{\chi^2 + 4\frac{g^2}{N}\psi^*\psi}}, \tag{13}$$

$$G(\psi^*,\psi) = \frac{1}{2}\sqrt{\chi^2 + 4\frac{g^2}{N}\psi^*\psi}, \tag{14}$$

with $\chi = \frac{\omega_0}{2} + \frac{U}{2N}\psi^*\psi$.

It is straightforward to find that the thermodynamic equilibrium equation (12) has two solutions. The trivial solution $\psi = \psi^* = 0$ corresponds to the NP, whereas the nontrivial solution $\psi(\tau) = \psi^*(\tau) = \pm\psi_0$, if it exists, governs the SP and satisfies the following nonlinear equation:

$$\frac{2\omega\zeta}{(\omega_0 + U\bar{\psi}_0^2)U + 8g^2} = \tanh\left(\frac{\beta\zeta}{4}\right), \tag{15}$$

where $\zeta = \sqrt{(\omega_0 + U\bar{\psi}_0^2)^2 + 16g^2\bar{\psi}_0^2}$ and $\bar{\psi}_0^2 = \langle\psi^\dagger\psi\rangle/N$ is the scaled mean-photon number. Moreover, the condition $\delta^2 S/\delta\psi^2$ (or $\delta^2 S/\delta(\psi^*)^2) > 0$ determines the stability of the solution of Eq. (12) and thus the phases of the BEC-cavity system at both zero and finite temperatures.

Before proceeding, we consider two limits. (i) For $U = 0$, i.e., the standard Dicke model, Eq. (15) reduces to the form

$$\frac{\omega}{4g^2}\sqrt{\omega_0^2 + 16g^2\bar{\psi}_0^2} = \tanh\left(\frac{\beta}{4}\sqrt{\omega_0^2 + 16g^2\bar{\psi}_0^2}\right). \tag{16}$$

In this case, only the SP and the NP can be found at both zero and finite temperatures, which is consistent with that of Ref. [38]. (ii) At zero temperature ($T = 0$), $\tanh(\beta\zeta/4) = 1$ and the scaled atomic population is thus given by $\langle S_z\rangle/2N = -1/2$ for the NP and

$$\frac{\langle S_z\rangle}{2N} = \frac{-\omega}{U} \pm \sqrt{\frac{g^2(4\omega^2 - U^2)}{U^2(4g^2 + U\omega_0)}} \tag{17}$$

for the SP, which are identical to those of Refs. [27,28]. With increasing temperature T, the function $\tanh(\beta\zeta/4)$ decreases. As a consequence, Eq. (15) possesses some new physical solutions, which can not only be used to explain the current experimental observation but also generate rich finite-temperature phase diagrams. In the following, we solve numerically the nonlinear equation (12), together with the stability condition, and then calculate the experimentally measurable mean-photon number $\langle\psi^\dagger\psi\rangle = N\bar{\psi}_0^2$.

IV. PHASE DIAGRAMS

A. The experimentally observed phase diagram

We first address the recent experimental observations of Esslinger's group. Using their experimental parameters [41],

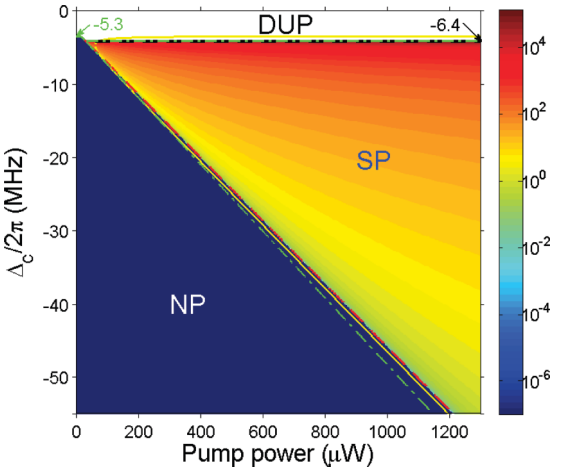

FIG. 2. (Color online) The mean-photon number $\langle\psi^\dagger\psi\rangle$ at $T = 50$ nk as a function of the pump-cavity detuning Δ_c and the pump power P based on the relation $g^2 \simeq 3.3\times10^{-3}P$ (MHz)^2. The nonlinear atom-photon interaction and the effective atomic frequency are given by $U = -2\pi \times 1.4$ MHz and $\omega_0 = 0.047$ MHz, respectively. In this figure, both red and black dashed lines, which describe the phase boundaries, are plotted in terms of our finite-temperature theory. However, the phase boundaries at $T = 0$ are shown in the green dash-dotted line (without decay of photon, our theory) and yellow solid line (with decay of photon, Ref. [26]), in order to have a clear comparison.

we have $g^2 \simeq 3.3\times10^{-3}P$ (MHz)^2 for $N = 1.0\times10^5$, where the unit of the pump power P is μW [42]. According to the above relation, we plot in Fig. 2 the mean-photon number $\langle\psi^\dagger\psi\rangle$ at $T = 50$ nK as a function of the pump-cavity detuning Δ_c and the pump power P. Since in experiment the nonlinear atom-photon interaction can reach the same order as other parameters, it affects strongly the stability condition and thus modifies significantly the phase diagrams. For example, due to the existence of this strong nonlinear atom-photon interaction, the effective cavity frequency is shifted to $\omega = -\Delta_c + 5U/2$. When $-\Delta_c < -5U/2$, we have $\omega < 0$ and $\delta^2 S/\delta\psi^2 < 0$ for both $\langle\psi^\dagger\psi\rangle = 0$ and $\langle\psi^\dagger\psi\rangle \neq 0$. In such a case there is no local minimum of the free energy of Hamiltonian (1) and the BEC-cavity system is unstable. We call the phase for $\omega < 0$ the DUP, in which no steady photon signal can be detected. This behavior is similar to the experimental observations [25]. However, there is a slight difference in the phase boundary (see the black dashed line in Fig. 2) since in the small $-\Delta_c$ regime the cavity loss ($\kappa = 8.1$ MHz in experiment) has a strong influence on it [27,28]. The transitions from the SP/NP to the DUP in Fig. 2 are only governed by variation of the second-order derivative of the free energy from $\delta^2 F/\delta\psi^2 > 0$ to $\delta^2 F/\delta\psi^2 < 0$. The other phase boundary (see the red dashed line in Fig. 2) is determined numerically from Eq. (15) and agrees well with the experimental observations. Moreover, our finite-temperature results are better than the zero-temperature predictions (see the green dash-dotted line and the yellow solid line in Fig. 2). Finally, we find that the magnitude of the mean-photon number $\langle\psi^\dagger\psi\rangle$ is almost identical to that of Ref. [25]. Based on the above analysis, we argue that the experimental observations of the Dicke phase transition can be better explained in terms of our finite-temperature theory.

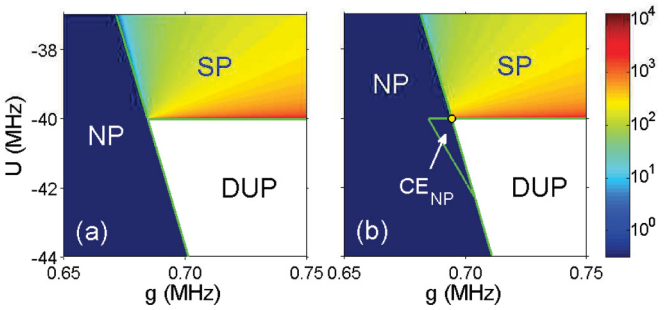

FIG. 3. (Color online) The mean-photon number $\langle\psi^\dagger\psi\rangle$ as a function of the collective coupling strength g and the nonlinear atom-photon interaction U for the different temperatures (a) $T = 0$ nK and (b) $T = 50$ nK with the effective cavity frequency $\omega = 20$ MHz and the effective atomic frequency $\omega_0 = 0.047$ MHz.

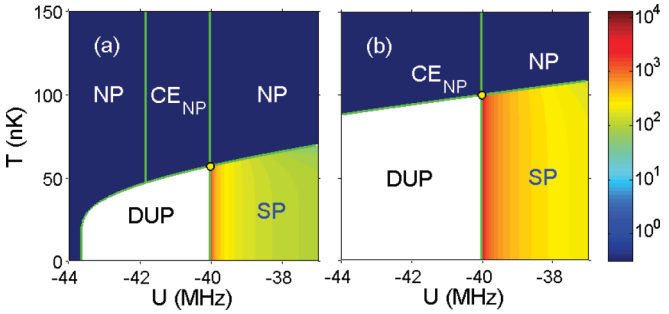

FIG. 4. (Color online) The mean-photon number $\langle\psi^\dagger\psi\rangle$ as a function of the nonlinear atom-photon interaction U and the temperature T for the different collective coupling strengths (a) $g = 0.70$ MHz and (b) $g = 0.75$ MHz with the effective cavity frequency $\omega = 20$ MHz and the effective atomic frequency $\omega_0 = 0.047$ MHz.

More importantly, we point out that a phase called the DUP can be identified in experiment.

B. The other phase diagrams

Having explained the experimental observations, we now explore the rich phase diagrams by varying the controllable parameters such as the pump-cavity detuning Δ_c, the collective coupling strength g, the nonlinear interaction U, and the temperature T. In Fig. 3, we plot the mean-photon number $\langle\psi^\dagger\psi\rangle$ as a function of the nonlinear interaction U and the collective coupling strength g for (a) $T = 0$ nK and (b) $T = 50$ nK. At finite temperature, a new phase called the $\mathrm{CE_{NP}}$ and a four-phase coexistence point emerge. In the so-called $\mathrm{CE_{NP}}$, both solutions of $\bar{\psi}_0^2 = 0$ and $\bar{\psi}_0^2 \neq 0$ of Eq. (12) satisfy the stability condition, which shows that two phases including the NP and the SP can coexist. On the other hand, the free energies for both $\bar{\psi}_0^2 = 0$ and $\bar{\psi}_0^2 \neq 0$ are obtained, respectively, by

$$\frac{F_{\mathrm{NP}}}{N} = -\frac{2}{\beta}\ln\left[2\cosh\left(\frac{\beta\omega_0}{4}\right)\right], \tag{18}$$

$$\frac{F_{\mathrm{SP}}}{N} = \omega|\bar{\psi}_0|^2 - \frac{2}{\beta}\ln\left[2\cosh\left(\frac{\beta\zeta}{4}\right)\right]. \tag{19}$$

Numerical simulation shows that $F_{\mathrm{NP}} < F_{\mathrm{SP}}$ in the $\mathrm{CE_{NP}}$, which implies that the NP is stable and the SP is metastable. Thus, the properties of the NP play the dominate role in determining the system's character, namely, a much weaker photon signature ($\langle\psi^\dagger\psi\rangle \to 0$) will be detected in the $\mathrm{CE_{NP}}$. However, it is quite different from the NP that the fluctuation of the free energy F in the $\mathrm{CE_{NP}}$ is much stronger due to the existence of the metastable SP. This means that in this $\mathrm{CE_{NP}}$, rich dynamics can occur [39]. In addition, the transition from the $\mathrm{CE_{NP}}$ to the SP/NP is a first-order phase transition. Whereas the phase transition from the $\mathrm{CE_{NP}}$ to the DUP belongs to an intrinsic transition, which is similar to the transition from the SP/NP to the DUP in Fig. 2.

Figure 4 plots the mean-photon number $\langle\psi^\dagger\psi\rangle$ as a function of the temperature T and the nonlinear atom-photon interaction U for the different collective coupling strengths (a) $g = 0.70$ MHz and (b) $g = 0.75$ MHz. It is shown that the many phase transitions and a four-phase coexistence point can be driven by adjusting the temperature T [43], if the nonlinear atom-photon interaction U and the collective coupling strength g are chosen to be appropriate values. The basic properties for the different phases are the same as those in Fig. 3. We note again that these exotic phase diagrams arise as results of the strong nonlinear atom-photon interaction U and the finite temperature T.

V. THE SPECIFIC HEAT

For a full understanding of the temperature-driven phase transitions, it is necessary to discuss the thermodynamic quantities in the different phases. Here we mainly consider the specific heat per atom defined as

$$C_V = \frac{1}{Nk_BT^2}\frac{\partial^2}{\partial\beta^2}(\ln Z). \tag{20}$$

The other thermodynamic quantities can be calculated via the same procedure. In the NP, the specific heat is obtained analytically by Ref. [18]

$$C_V^{\mathrm{NP}} = \frac{\omega_0^2}{8k_BT^2}\left[1 - \tanh^2\left(\frac{\beta\omega_0}{4}\right)\right], \tag{21}$$

which reaches maximum at a certain temperature (see the blue dashed line in Fig. 5). However, the explicit expression for the specific heat in the SP cannot be obtained analytically in general. Nevertheless, in the region $T \ll T_c$, where T_c is the critical temperature separating the SP from the NP, we find

$$C_V^{\mathrm{SP}} \simeq \frac{\zeta_0^2}{8k_BT^2}\mathrm{sech}^2\left(\frac{\zeta_0}{4k_BT}\right), \tag{22}$$

where ζ_0 is the value of $\zeta = \sqrt{(\omega_0 + U\bar{\psi}_0^2)^2 + 16g^2\bar{\psi}_0^2}$ at $T = 0$. This analytical expression agrees well with the numerical simulation, as shown in the insert part of Fig. 5. According to Eq. (22), we find that the specific heat in the SP increases exponentially at lower temperatures. More interestingly, the specific heat has a large jump at the critical temperature T_c (see the red dash-dotted line of Fig. 5). This jump behavior is quite different from that of the mean-photon number $\langle\psi^\dagger\psi\rangle$, which varies smoothly across the critical point. Therefore the temperature-driven phase transition can be detected by measuring the specific heat.

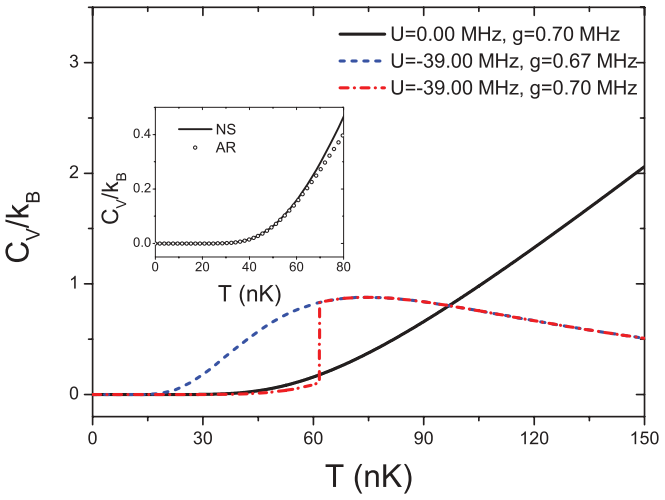

FIG. 5. (Color online) The specific heat C_V as a function of the temperature T for the different nonlinear atom-photon interactions U and the collective coupling strengths g, where the effective cavity frequency and the effective atomic frequency are given by $\omega = 20$ MHz and $\omega_0 = 0.047$ MHz, respectively. Insert: The comparison of the analytical result (AR) of the specific heat C_V in Eq. (22) with the direct numerical simulation (NS).

VI. CONCLUSIONS

In summary, we have developed a finite-temperature theory for the recent experiment of the BEC-cavity system with the strong nonlinear atom-photon interaction. Our theory has not only explained the experimental observation of the Dicke phase transition from the NP to the SP but also has predicted rich new phases that either have been observed (but not pointed out) or may be observable by tuning experimental parameters to appropriate regimes. Our study is of crucial importance for understanding the Dicke phase transition in a realistic experimental system and may have potential applications in quantum simulation, quantum optics, etc.

ACKNOWLEDGMENTS

We thank Professor T. Esslinger, Professor Jing Zhang, Dr. K. Baumann, Dr. F. Brennecke, Dr. Yongping Zhang, and Dr. Ming Gong for helpful discussions and suggestions. This work is supported by the 973 Program under Grant No. 2012CB921603, the NNSFC under Grants No. 10934004, No. 60978018, No. 61008012, No. 11074154, No. 11075099, No. 11275118, and No. 61275211. C.Z. is supported by the NSF.

[1] F. Brennecke, T. Donner, S. Ritter, T. Bourdel, M. Köhl, and T. Esslinger, Nature (London) **450**, 268 (2007).
[2] Y. Colombe, T. Steinmetz, G. Dubois, F. Linke, D. Hunger, and J. Reichel, Nature (London) **450**, 272 (2007).
[3] C. Maschler and H. Ritsch, Phys. Rev. Lett. **95**, 260401 (2005).
[4] D. Nagy, J. K. Asbóth, P. Domokos, and H. Ritsch, Europhys. Lett. **74**, 254 (2006); D. Nagy, G. Szirmai, and P. Domokos, Eur. Phys. J. D **48**, 127 (2008).
[5] J. M. Zhang, W. M. Liu, and D. L. Zhou, Phys. Rev. A **78**, 043618 (2008).
[6] S. Morrison and A. S. Parkins, Phys. Rev. Lett. **100**, 040403 (2008); Phys. Rev. A **77**, 043810 (2008).
[7] J. Larson, B. Damski, G. Morigi, and M. Lewenstein, Phys. Rev. Lett. **100**, 050401 (2008); J. Larson and M. Lewenstein, New J. Phys. **11**, 063027 (2009); J. Larson and J.-P. Martikainen, Phys. Rev. A **82**, 033606 (2010).
[8] S. Gopalakrishnan, B. L. Lev, and P. M. Goldbart, Nat. Phys. **5**, 845 (2009); Phys. Rev. Lett. **107**, 277201 (2011).
[9] L. Zhou, H. Pu, H. Y. Ling, K. Zhang, and W. Zhang, Phys. Rev. Lett. **103**, 160403 (2009); L. Zhou, H. Pu, H. Y. Ling, and W. Zhang, Phys. Rev. A **81**, 063641 (2010).
[10] M. J. Bhaseen, M. Hohenadler, A. O. Silver, and B. D. Simons, Phys. Rev. Lett. **102**, 135301 (2009); A. O. Silver, M. Hohenadler, M. J. Bhaseen, and B. D. Simons, Phys. Rev. A **81**, 023617 (2010).
[11] G. Szirmai, D. Nagy, and P. Domokos, Phys. Rev. Lett. **102**, 080401 (2009); Phys. Rev. A **81**, 043639 (2010).
[12] S. Fernández-Vidal, G. De Chiara, J. Larson, and G. Morigi, Phys. Rev. A **81**, 043407 (2010).
[13] P. Strack and S. Sachdev, Phys. Rev. Lett. **107**, 277202 (2011).
[14] V. M. Bastidas, C. Emary, B. Regler, and T. Brandes, Phys. Rev. Lett. **108**, 043003 (2012).
[15] F. Brennecke, S. Ritter, T. Donner, and T. Esslinger, Science **322**, 235 (2008).
[16] T. P. Purdy, D. W. C. Brooks, T. Botter, N. Brahms, Z.-Y. Ma, and D. M. Stamper-Kurn, Phys. Rev. Lett. **105**, 133602 (2010).
[17] R. H. Dicke, Phys. Rev. **93**, 99 (1954).
[18] K. Hepp and E. H. Lieb, Ann. Phys. (NY) **76**, 360 (1973).
[19] Y. K. Wang and F. T. Hioes, Phys. Rev. A **7**, 831 (1973).
[20] F. T. Hioes, Phys. Rev. A **8**, 1440 (1973).
[21] C. Emary and T. Brandes, Phys. Rev. E **67**, 066203 (2003).
[22] F. Dimer, B. Estienne, A. S. Parkins, and H. J. Carmichael, Phys. Rev. A **75**, 013804 (2007).
[23] G. Chen, Xiaoguang Wang, J.-Q. Liang, and Z. D. Wang, Phys. Rev. A **78**, 023634 (2008).
[24] D. Nagy, G. Kónya, G. Szirmai, and P. Domokos, Phys. Rev. Lett. **104**, 130401 (2010).
[25] K. Baumann, C. Guerlin, F. Brennecke, and T. Esslinger, Nature (London) **464**, 1301 (2010).
[26] K. Baumann, R. Mottl, F. Brennecke, and T. Esslinger, Phys. Rev. Lett. **107**, 140402 (2011).
[27] J. Keeling, M. J. Bhaseen, and B. D. Simons, Phys. Rev. Lett. **105**, 043001 (2010).
[28] M. J. Bhaseen, J. Mayoh, B. D. Simons, and J. Keeling, Phys. Rev. A **85**, 013817 (2012).
[29] N. Liu, J. Lian, J. Ma, L. Xiao, G. Chen, J.-Q. Liang, and S. Jia, Phys. Rev. A **83**, 033601 (2011).
[30] S. Sachdev, *Quantum Phase Transtitions* (Cambridge University Press, Cambridge, 1999).
[31] A. Griffin, T. Nikuni, and E. Zaremba, *Bose-Condensed Gases at Finite Temperatures* (Cambridge University Press, Cambridge, 2009).
[32] P. C. Hohenberg, Phys. Rev. **158**, 383 (1967).

[33] V. L. Berezinskii, Sov. Phys. JETP **32**, 493 (1971).
[34] J. M. Kosterlitz and D. Thouless, J. Phys. C **5**, L124 (1972); **6**, 1181 (1973).
[35] P. Nataf and C. Ciuti, Nat. Commun. **1**, 72 (2010).
[36] O. Viehmann, J. von Delft, and F. Marquardt, Phys. Rev. Lett. **107**, 113602 (2011).
[37] The coefficients have been revised slightly, compared with the experimental Hamiltonian. The detailed calculations are given in Appendix A of Ref. [28].
[38] V. N. Popov and S. A. Fedotov, Theor. Math. Phys. **51**, 363 (1982).
[39] A. Altland and B. Simons, *Condensed Matter Field Theory* (Cambridge University Press, Cambridge, 2010).
[40] R. D. Mattuck, *A Guide to Feynman Diagrams in the Many-Body Problem* (Dover, New York, 1976), p. 251.
[41] In Ref. [25], the length for the high-finesse optical cavity is $L = 178$ μm and the waist radius of the cavity TM_{00} mode is $w_c = 25$ μm. Thus, the transition dipole matrix element and the single atom-photon coupling strength are evaluated as $D = 3.58 \times 10^{-29}$ C·m and $g_0 = 2\pi \times 14.11$ MHz, respectively. In addition, the wavelength of the pump laser is $\lambda_P = 784.5$ nm. Moreover, it is red-detuned by 4.3 nm from the atom D_2 line.
[42] S. M. Dutra, *Cavity Quantum Electrodynamics: The Strange Theory of Light in a Box* (Wiley & Sons, New Jersey, 2005).
[43] F. Dalfovo, S. Giorgini, L. P. Pitaevskii, and S. Stringari, Rev. Mod. Phys. **71**, 463 (1999).